Optics Letters

Spontaneous four-wave mixing in silicon nitride waveguides for broadband coherent anti-Stokes Raman scattering spectroscopy

Niklas M. Lüpken,[1,*,†] Thomas Würthwein,[1,†] Jörn P. Epping,[2] Klaus-J. Boller,[1,3] and Carsten Fallnich[1,3]

[1]Institute of Applied Physics, University of Münster, Corrensstraße 2, 48149 Münster, Germany
[2]LioniX International B.V., P.O. Box 456, Enschede 7500 AL, The Netherlands
[3]MESA+ Institute for Nanotechnology, University of Twente, P.O. Box 217, Enschede 7500 AE, The Netherlands
*Corresponding author: n.luepken@uni-muenster.de

Received 28 April 2020; revised 4 June 2020; accepted 4 June 2020; posted 8 June 2020 (Doc. ID 396394); published 6 July 2020

We present a light source for coherent anti-Stokes Raman scattering (CARS) based on broadband spontaneous four-wave mixing, with the potential to be further integrated. By using 7 mm long silicon nitride waveguides, which offer tight mode confinement and a high nonlinear refractive index coefficient, broadband signal and idler pulses were generated with 4 nJ of input pulse energy. In comparison to fiber-based experiments, the input energy and the waveguide length were reduced by two orders of magnitude, respectively. The idler and residual pump pulses were used for CARS measurements, enabling chemically selective and label-free spectroscopy over the entire fingerprint region, with an ultrafast fiber-based pump source at 1033 nm wavelength. The presented simple light source paves the path towards cost-effective, integrated lab-on-a-chip CARS applications.

https://doi.org/10.1364/OL.396394

Coherent anti-Stokes Raman scattering (CARS) enables a label-free, non-destructive, and chemically selective contrast in spectroscopic imaging, which is of high interest for many biomedical applications [1], such as tissue tomography [2] or investigations of cell biology [3]. As the CARS process relies on the coherent excitation of a molecular resonance with the frequency Ω, two excitation beams with different frequencies ω_i have to be used, such that the resonance condition $\omega_2 - \omega_1 = \Omega$ is fulfilled. These frequencies are typically generated by a mode-locked laser in combination with an optical parametric oscillator (OPO), which is a versatile but expensive and large device, and typically critical to align and to maintain [4]. Due to the high required pump powers, these systems become big and complex; hence, CARS microscopy is still restricted to specialized laboratories, when using mode-locked lasers and OPOs.

Fiber-based light sources allow to overcome many of these problems, as they can be compact including dual-color output and, therefore, show great applicability for CARS microscopy. The dual-color output can be achieved by nonlinear frequency conversion in photonic crystal fibers (PCFs) within fiber-based OPOs [5–8] or other four-wave mixing (FWM) schemes [9,10]. However, high pulse energies are required on account of low fiber nonlinearity, resulting in a light source size that does not allow integration for on-chip Raman spectroscopy [11,12].

In contrast to optical fibers, the integrated silicon nitride (Si_3N_4) platform offers a small footprint and CMOS compatibility, enabling cheap and scalable fabrication [13]. Furthermore, these waveguides provide an increased nonlinearity compared to optical fibers due to the tighter mode confinement and higher nonlinear refractive index coefficient, rendering them ideal for efficiently driving nonlinear processes, e.g., supercontinuum generation [14,15] or frequency comb generation [16,17]. Efficient FWM in Si_3N_4 waveguides was already demonstrated; however, the generated frequencies did not provide suitable energy differences Ω for CARS measurements, as the frequency conversion was restricted to the telecommunication band [18] or to the mid-infrared wavelength region [19].

In this Letter, we present a simple light source for broadband CARS spectroscopy based on broadband spontaneous FWM in Si_3N_4 waveguides with an ultrafast fiber-based pump source. Our light source requires two orders of magnitude lower optical pump power in comparison to experiments in PCFs [9,10]. The simple, integrated frequency conversion module enables the CARS measurements and paves the path towards integrated, lab-on-a-chip CARS applications. The measurement scheme works as follows: a narrowband pump beam [see Fig. 1(a)] is launched into a Si_3N_4 waveguide, wherein signal and idler sidebands are generated via degenerate FWM [see Fig. 1(b)]. The residual pump and the idler beam [see Fig. 1(c)] are focused into a sample to excite a CARS signal, which is detected by means of a spectrometer [see Fig. 1(d)].

In spontaneous degenerate FWM, two pump photons with angular frequency ω_p are annihilated, and a signal and an idler photon with angular frequencies ω_s and ω_i, respectively, are generated. In order to efficiently drive this FWM process, the energy conservation $2\omega_p = \omega_s + \omega_i$ and the phase-matching condition $\Delta k = 2\beta_p - \beta_s - \beta_i = 0$ have to be fulfilled, where β_j are the

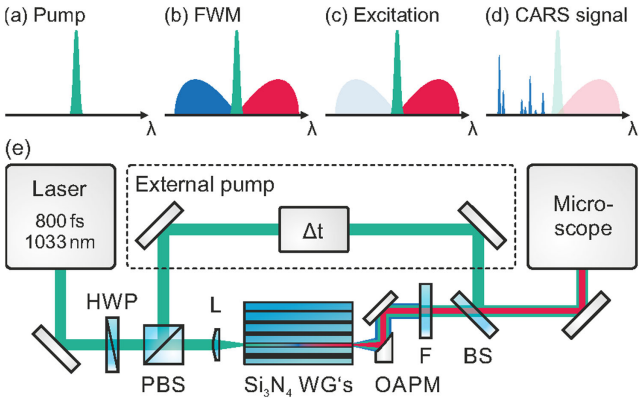

Fig. 1. Schematics of the spectral components of (a) pump beam, (b) waveguide output, (c) excitation beam incident onto the sample, and (d) generated CARS signal. (e) Schematic setup of CARS measurements driven by a FWM light source. For details, see text.

propagation constants with $j = \mathrm{p, s, i}$. The parametric gain of FWM is given as [20]

$$g = \sqrt{(\gamma P_0)^2 - (\kappa/2)^2}, \tag{1}$$

where $\kappa = \Delta k + 2\gamma P_0$ is the effective phase mismatch, P_0 the peak power of the pump beam, and $\gamma = n_2\omega_\mathrm{p}/(cA_\mathrm{eff}) \approx 1(\mathrm{Wm})^{-1}$ the nonlinear coefficient with the nonlinear refractive index coefficient n_2, the speed of light c, and the effective mode area A_eff.

We calculated the frequency-dependent parametric gain $g(\omega)$ according to Eq. (1) for Si_3N_4 waveguides with a height of 950 nm and different widths ranging from 800 nm to 1500 nm by calculating the dispersion $\beta(\omega)$ for each waveguide with a commercial mode solver (FIMMWAVE by Photon Design). For this purpose, the Sellmeier equation for Si_3N_4 published in Ref. [16] was used. The calculated parametric gain for a peak power of 550 W is shown color-coded as a function of the wavelength and of the waveguide width in Fig. 2(b); and four exemplary gain curves are plotted in Fig. 2(a). The parametric gain broadens but decreases with increasing waveguide width, until a waveguide width is reached where the pump wavelength lies in the normal dispersion regime, thus exhibiting no parametric FWM gain. In order to use these FWM sidebands for CARS measurements, either the fingerprint region ($<1800\ \mathrm{cm}^{-1}$) or the C–H-stretch region ($2800\ \mathrm{cm}^{-1}$–$3200\ \mathrm{cm}^{-1}$) has to be accessed. Here, a waveguide with a width of 1300 nm was chosen for sufficient gain and bandwidth to address the fingerprint region [see Fig. 2(a)], which features many different molecule-specific Raman resonances. Other wavelength regions can be accessed by engineering the dispersion via different cross sections [19], e.g., for addressing the C–H-stretch region in future experiments.

The experimental setup is shown in Fig. 1(e). An ytterbium-doped fiber laser emitted pulses with a pulse duration of 800 fs centered at 1033 nm wavelength with a repetition rate of 1 MHz. These pulses were split into two copies with a half-wave plate (HWP) and a polarizing beam-splitter (PBS). One pulse copy was launched with an aspherical lens (L) into a 7 mm long Si_3N_4 waveguide (provided by LioniX International B.V.), wherein signal and idler sidebands were generated via FWM. An off-axis parabolic mirror (OAPM) was used for collimating the

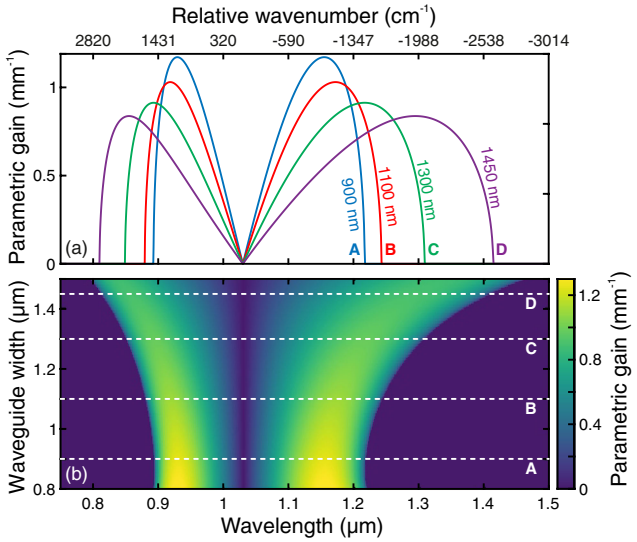

Fig. 2. (a) Parametric FWM gain in a Si_3N_4 waveguide with a height of 950 nm calculated as a function of the wavelength for four exemplary waveguide widths [compare with cuts A–D from (b)]. (b) Parametric FWM gain as a function of the wavelength and of the waveguide width.

output, and a subsequent long-pass filter (F) removed the signal sideband. The second copy of the pump pulse was bypassed around the waveguide. This external pump beam served as a reference and was overlapped spatially at a 70:30 beam splitter (BS, 70% transmission) with the light beam emerging from the waveguide. Temporal overlap was ensured with a delay line (Δt). Both beams were guided to a home-built microscope, where they were focused into a sample using a microscope objective (NA = 0.6). The emerging beams were collected using a second microscope objective (NA = 0.6), and a short-pass filter transmitted only the CARS signal generated inside the sample to a spectrometer.

In order to characterize the spectral power distribution of the idler sideband generated by FWM, the spectrum of the light emerging from the waveguides output was measured. The measured output FWM spectra are depicted in Fig. 3(a) for input pulse energies ranging from 2 nJ to 4 nJ (solid lines), which were well below the damage threshold of the waveguide of about 10 nJ. The two signal and idler sidebands are clearly visible and cover a spectral range from 850 nm to 1300 nm at 4 nJ input energy, which is in agreement with the phase-matching calculations [see Fig. 2(a)] and sufficient for CARS measurements in the fingerprint region. The output spectra of wider and narrower waveguides matched the phase-matching condition as well; however, the used waveguide width provided the best trade-off between bandwidth and spectral power density for CARS measurements. With increasing pump pulse energy, the bandwidth of these sidebands became broader, and the distance of the peak wavelength to the pump wavelength increased, which is the result of the nonlinear phase shift γP_0 [compare Eq. (1)]. Furthermore, the output energy of the signal and idler sidebands increased exponentially, which is in agreement with theory [20]. The maximum output pulse energy of each sideband was approximately 15 pJ, limited by the used pump pulse energy, which was restricted by the damage threshold. This output energy corresponded to an external conversion efficiency

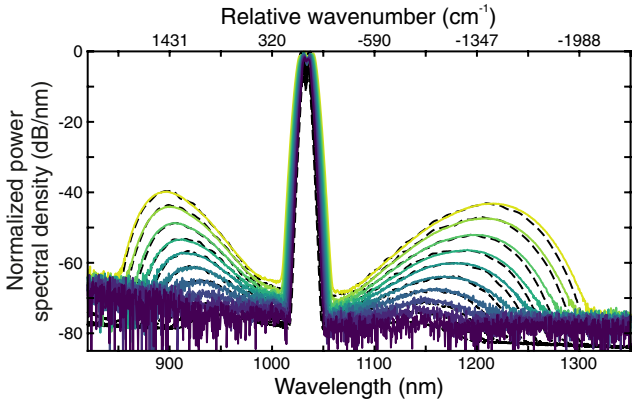

Fig. 3. Spontaneous FWM spectra in a Si_3N_4 waveguide with a height of 950 nm and a width of 1300 nm for different input energies (solid lines from violet, 2 nJ, to yellow, 4 nJ). Corresponding simulations are depicted as dashed lines.

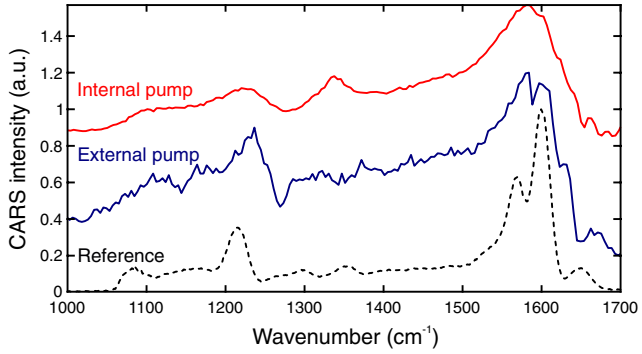

Fig. 4. CARS spectra of cinnamomum cassia oil measured with an external pump beam (blue curve) and the residual internal waveguide pump beam (red curve). The black dashed curve shows a CARS spectrum measured with the fiber-based optical parametric oscillator from Ref. [6]. The spectra were shifted vertically for better visibility.

of −24.3 dB, which is comparable to the results in Refs. [18,19] when taking the differences of waveguide length and pump energy into account. The achieved energies are sufficient for CARS spectroscopy, but are not suitable for high-speed imaging applications [8].

In order to get a better understanding of the FWM process, corresponding simulations were performed based on the nonlinear Schrödinger equation of Ref. [21]. For a best fit to the experimental spectra, the launched pulse energy in the simulations was adjusted to the experiments with a coupling constant of about 36%. This value compares well to experimental estimations as well as coupling efficiencies achieved in earlier work with the same type of waveguides [15]. The simulation results, shown as dashed lines in Fig. 3, reveal an excellent agreement with the experimental data in terms of spectral shape and bandwidth. This agreement between the simulations as well as the phase-matching condition with the experimental data proves a high reliability in calculating the propagation constants for the used Si_3N_4 waveguides. Therefore, the phase-matching condition can be used to predict the generated spectra and output powers also for other waveguide geometries, for addressing other spectral regions, such as the C–H-stretch region, or for increasing the bandwidth of the output FWM sidebands.

In order to use the FWM source for CARS measurements, the signal sideband was removed with a long-pass filter and CARS spectra were acquired using a home-built microscope with the pump beam at 1033 nm and the idler sideband generated by FWM as the Stokes beam. Figure 4 shows the measured CARS spectra of a cinnamomum cassia oil sample. A reference spectrum, depicted as a black dashed curve, was measured with a fiber-based OPO as described in Ref. [6]. The blue curve shows the CARS spectrum measured with the idler sideband in combination with the external reference pump beam, which was bypassed around the waveguide with a pulse energy of 4 nJ. The Raman resonances are clearly visible and show the characteristic dispersive lineshapes [1]. However, the double resonance around 1600 cm^{-1} is hardly resolved due to the spectral resolution of approx. 36 cm^{-1}, limited by the spectral bandwidth of the pump pulses. In future experiments, this could be improved by using pump pulses with a narrower spectral bandwidth, e.g., bandwidth-limited 1 ps pulses would allow for a spectral resolution of 15 cm^{-1}, which should be sufficient for most CARS applications.

In order to simply use the waveguide output to stimulate the CARS process and avoid any external delay lines, it is desirable to acquire CARS spectra without bypassing an external pump beam around the waveguide. For this purpose, a CARS spectrum was measured only with the light emerging from the waveguide, i.e., the idler sideband and the residual pump beam, when pumped with 4 nJ pulse energy. The measured spectrum is shown as a red curve in Fig. 4. This CARS spectrum shows the main spectral features of the sample. However, the spectral resolution is decreased to roughly 55 cm^{-1} due to a spectrally broadened pump beam on account of self-phase modulation. Therefore, the double resonance around 1600 cm^{-1} is not resolved. In future experiments, the spectral resolution could be improved by proper pre-chirping of the pump pulses, leading to spectral narrowing by self-phase modulation [22].

Nonetheless, the light emerging from the waveguide was strong enough to enable chemical contrast by CARS. In comparison to similar experiments using spontaneous FWM in PCFs, our experiment in Si_3N_4 waveguides required two orders of magnitude less pump energy and a two orders of magnitude shorter waveguide [9].

In order to determine the distinguishability of the measured spectral signatures in the fingerprint region, CARS spectra were acquired (blues curves in Fig. 5) for a representative selection of chemicals typically appearing in spectroscopy, namely, cyclohexane, cyclohexanon, ethanol, immersol, and rapeseed oil. An external pump beam with a pulse energy of about 4 nJ was used, and the integration time of the spectrometer was set to 1 s. Related spontaneous Raman scattering spectra (gray curves in Fig. 5) were acquired as a reference using a home-built setup described in Ref. [23]. From all CARS spectra, the dark count spectrum was subtracted, and to account for the spectral shape of the idler, all CARS spectra were divided by the idler spectrum (converted to wavenumbers). The CARS spectra again show the dispersive lineshapes, typical for CARS resonances, with a spectral resolution of about 36 cm^{-1}, limited by the spectral width of the pump pulses. The vertical dashed lines in Fig. 5 mark the salient Raman resonances in the reference spectra, which were also clearly visible in the measured CARS spectra.

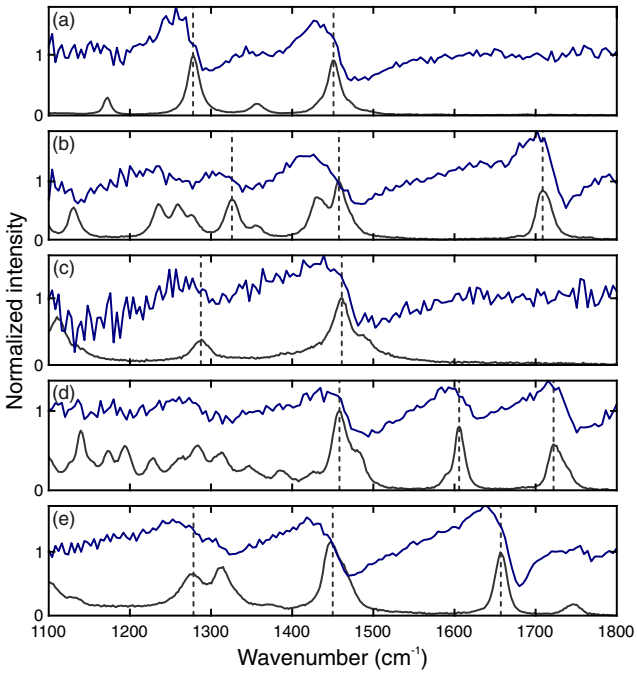

Fig. 5. Measured CARS spectra (blue curves) of (a) cyclohexane, (b) cyclohexanone, (c) ethanol, (d) immersol, and (e) rapeseed oil. Corresponding spontaneous Raman scattering spectra are added as a reference (gray curves). The dashed lines mark salient resonances.

However, weaker Raman resonances [e.g., at 1288 cm^{-1} in Fig. 5(c)] could not be resolved due to a low signal-to-noise ratio on account of the low energy levels and integration times used here. Nevertheless, the spectra of the measured samples became clearly and unambiguously distinguishable with the light generated by spontaneous FWM, making the demonstrated approach suitable for future on-chip CARS applications in the fingerprint region.

In summary, we have demonstrated a light source based on spontaneous FWM for broadband CARS in the fingerprint region with the potential to be further integrated. Signal and idler pulses were generated in a 7 mm long Si_3N_4 waveguide with only 4 nJ of pump pulse energy, which corresponds to an improvement by two orders of magnitude with respect to the input pulse energy as well as the waveguide length, respectively, compared to fiber experiments [9]. After removing the signal beam, the residual idler and pump beams were used to acquire CARS spectra in a home-built microscope. The presented light source allowed the distinguishability of different liquid samples by their distinct CARS spectra.

In future experiments, the chemical specificity of the presented proof-of-principle setup can be enhanced by improvements regarding the contrast and spectral resolution. Longer pump pulse durations will enhance the spectral resolution of the CARS spectra. In order to reduce the necessary input energy or to increase the output energy, a longer waveguide (longer than the available 7 mm) could be used, as the FWM signal scales exponentially with the length of the waveguide. Furthermore, a simple, continuous-wave, and narrowband seed in the signal band should increase the FWM conversion efficiency by orders of magnitude and enhance the spectral resolution simultaneously [10,19]. Furthermore, by integrating the seed source [24], the spectrometer [25] and the samples within microfluidic channels [26] or via evanescent field sensing [12], on-chip CARS applications will be enabled.

Disclosures. The authors declare no conflicts of interest.

[†]These authors contributed equally to this work.

REFERENCES

1. C. L. Evans and X. S. Xie, Annu. Rev. Anal. Chem. **1**, 883 (2008).
2. C. L. Evans, E. O. Potma, M. Puoris'haag, D. Cote, C. P. Lin, and X. S. Xie, Proc. Natl. Acad. Sci. **102**, 16807 (2005).
3. J.-X. Cheng, Y. K. Jia, G. Zheng, and X. S. Xie, Biophys. J. **83**, 502 (2002).
4. M. Jurna, J. P. Korterik, H. L. Offerhaus, and C. Otto, Appl. Phys. Lett. **89**, 251116 (2006).
5. J. E. Sharping, J. Lightwave Technol. **26**, 2184 (2008).
6. M. Brinkmann, S. Janfrüchte, T. Hellwig, S. Dobner, and C. Fallnich, Opt. Lett. **41**, 2193 (2016).
7. K. Yang, S. Zheng, Y. Wu, P. Ye, K. Huang, Q. Hao, and H. Zeng, Opt. Express **26**, 17519 (2018).
8. M. Brinkmann, A. Fast, T. Hellwig, I. Pence, C. L. Evans, and C. Fallnich, Biomed. Opt. Express **10**, 4437 (2019).
9. M. Baumgartl, M. Chemnitz, C. Jauregui, T. Meyer, B. Dietzek, J. Popp, J. Limpert, and A. Tünnermann, Opt. Express **20**, 4484 (2012).
10. S. Lefrancois, D. Fu, G. R. Holtom, L. Kong, W. J. Wadsworth, P. Schneider, R. Herda, A. Zach, X. Sunney Xie, and F. W. Wise, Opt. Lett. **37**, 1652 (2012).
11. C. H. Camp, Jr., S. Yegnanarayanan, A. A. Eftekhar, H. Sridhar, and A. Adibi, Opt. Express **17**, 22879 (2009).
12. A. Dhakal, A. Z. Subramanian, P. Wuytens, F. Peyskens, N. L. Thomas, and R. Baets, Opt. Lett. **39**, 4025 (2014).
13. J. P. Epping, M. Hoekman, R. Mateman, A. Leinse, R. G. Heideman, A. van Rees, P. J. van der Slot, C. J. Lee, and K.-J. Boller, Opt. Express **23**, 642 (2015).
14. J. P. Epping, T. Hellwig, M. Hoekman, R. Mateman, A. Leinse, R. G. Heideman, A. van Rees, P. J. van der Slot, C. J. Lee, C. Fallnich, and K.-J. Boller, Opt. Express **23**, 19596 (2015).
15. M. A. G. Porcel, F. Schepers, J. P. Epping, T. Hellwig, M. Hoekman, R. G. Heideman, P. J. M. van der Slot, C. J. Lee, R. Schmidt, R. Bratschitsch, C. Fallnich, and K.-J. Boller, Opt. Express **25**, 1542 (2017).
16. K. Luke, Y. Okawachi, M. R. E. Lamont, A. L. Gaeta, and M. Lipson, Opt. Lett. **40**, 4823 (2015).
17. A. L. Gaeta, M. Lipson, and T. J. Kippenberg, Nat. Photonics **13**, 158 (2019).
18. J. S. Levy, A. Gondarenko, A. C. Turner-Foster, M. A. Foster, A. L. Gaeta, and M. Lipson, in *Conf. Lasers Electro-Optics/International Quantum Electron. Conf.* (Optical Society of America, 2009), paper CMFF5.
19. A. S. Kowligy, D. D. Hickstein, A. Lind, D. R. Carlson, H. Timmers, N. Nader, D. L. Maser, D. Westly, K. Srinivasan, S. B. Papp, and S. A. Diddams, Opt. Lett. **43**, 4220 (2018).
20. G. Agrawal, *Nonlinear Fiber Optics*, 5th ed. (Academic, 2013).
21. F. Poletti and P. Horak, J. Opt. Soc. Am. B **25**, 1645 (2008).
22. S. A. Planas, N. L. Pires Mansur, C. H. Brito Cruz, and H. L. Fragnito, Opt. Lett. **18**, 699 (1993).
23. S. Rieger, D. Grill, V. Gerke, and C. Fallnich, J. Raman Spectrosc. **48**, 1264 (2017).
24. K. Franken, A. van Rees, Y. Fan, D. Geskus, R. Dekker, D. Geuzebroek, C. Fallnich, P. van der Slot, and K.-J. Boller, Proc. SPIE **11301**, 1130106 (2020).
25. X. Nie, E. Ryckeboer, G. Roelkens, and R. Baets, Opt. Express **25**, A409 (2017).
26. K. Wörhoff, R. G. Heideman, A. Leinse, and M. Hoekman, Adv. Opt. Technol. **4**, 189 (2015).